# UNIVERSITY *of York*

This is a repository copy of *Statistical study of the prompt-fission γ -ray spectrum for U 238 (n, f) in the fast-neutron region STATISTICAL STUDY of the PROMPT-FISSION ... L. QI et al.*.

# Statistical study of the prompt-fission $\gamma$-ray spectrum for $^{238}$U($n, f$) in the fast-neutron region

L. Qi,[1] M. Lebois,[1,*] J. N. Wilson,[1] A. Chatillon,[2] S. Courtin,[3] G. Fruet,[3] G. Georgiev,[4] D. G. Jenkins,[5] B. Laurent,[2]
L. Le Meur,[6] A. Maj,[7] P. Marini,[2] I. Matea,[1] L. Morris,[5] V. Nanal,[8] P. Napiorkowski,[9] A. Oberstedt,[10] S. Oberstedt,[11]
C. Schmitt,[12] O. Serot,[13] M. Stanoiu,[14] and B. Wasilewska[7]

[1]*Institut de Physique Nucléaire, CNRS-IN2P3, Univ. Paris-Sud, Université Paris-Saclay, 91406 Orsay Cedex, France*
[2]*CEA, DAM, DIF, F-91297 Arpajon, France*
[3]*Université de Strasbourg, IPHC, 23 rue du Loess, 67037 Strasbourg, France*
*and CNRS, UMR7178, 67037 Strasbourg, France*
[4]*CSNSM Orsay, CNRS-IN2P3, Université Paris-Sud, Université Paris-Saclay, 91405 Orsay Cedex, France*
[5]*Department of Physics, University of York, Heslington, York YO10 5DD, United Kingdom*
[6]*Subatech, IMT-Atlantique, rue Alfred Kastler 4, 44307 Nantes, France*
[7]*The Henryk Niewodniczański Institute of Nuclear Physics, 31-342 Krakow, Poland*
[8]*Department of Nuclear and Atomic Physics, Tata Institute of Fundamental Research, Mumbai -5, India*
[9]*Heavy Ion Laboratory, University of Warsaw, Poland*
[10]*Extreme Light Infrastructure-Nuclear Physics (ELI-NP)/Horia Hulubei National Institute for Physics and Nuclear Engineering (IFIN-HH),
077125 Bucharest-Magurele, Romania*
[11]*European Commission, Joint Research Centre, Directorate G for Nuclear Safety and Security, Unit G.2, 2440 Geel, Belgium*
[12]*Grand Accélérateur National d'Ions Lourd, Bd Henri Becquerel, BP 55027 - 14076 CAEN Cedex 05, France*
[13]*CEA, DEN, DER, SPRC, Physics Studies Laboratory, Cadarache, F-13108 Saint Paul Lez Durance, France*
[14]*Institute of Atomic Physics, IFIN-HH, Bucharest-Magurele, P.O. Box MG6, Romania*

Prompt-fission $\gamma$-ray spectra (PFGS) have been measured for the $^{238}$U($n, f$) reaction using fast neutrons produced by the LICORNE directional neutron source. Fission events were detected with an ionization chamber containing actinide samples placed in the neutron beam, and the coincident prompt-fission $\gamma$ rays were measured using a number of LaBr$_3$ scintillation detectors and a cluster of nine phoswich detectors from the PARIS array. Prompt-fission $\gamma$ rays (PFGs) were discriminated from prompt-fission neutrons using the time-of-flight technique over distances of around 35 cm. PFG emission spectra were measured at two incident neutron energies of 1.9 and 4.8 MeV for $^{238}$U($n, f$) and also for $^{252}$Cf($sf$) as a reference. Spectral characteristics of PFG emission, such as mean $\gamma$ multiplicity and average total $\gamma$-ray energy per fission, as well as the average $\gamma$-ray energy, were extracted. The sensitivity of these results to the width of the time window and the type of spectral unfolding procedure used to correct for the detector responses was studied. Iteration methods were found to be more stable in low-statistics data sets. The measured values at $E_n = 1.9$ MeV were found to be the mean $\gamma$ multiplicity $\overline{M}_\gamma = 6.54 \pm 0.19$, total released energy per fission $E_{\gamma,\text{tot}} = 5.25 \pm 0.20$ MeV, and the average $\gamma$-ray energy $\epsilon_\gamma = 0.80 \pm 0.04$ MeV. Under similar conditions, the values at $E_n = 4.8$ MeV were measured to be $\overline{M}_\gamma = 7.31 \pm 0.46$, $E_{\gamma,\text{tot}} = 6.18 \pm 0.65$ MeV, and $\epsilon_\gamma = 0.84 \pm 0.11$ MeV.

## I. INTRODUCTION

In recent years, the development of Generation IV reactors revived the measurement of prompt-fission $\gamma$-ray spectra (PFGS), namely spectral characteristics such as $\gamma$-ray multiplicity, total $\gamma$-ray energy release, and average photon energy, for different fissioning systems. These are crucial nuclear data needed, e.g., as input for $\gamma$ heating calculations in reactor physics. In some recent reactor experiments, $\gamma$ heating was shown to be underestimated by up to 28% [1]. Moreover, for three types of Generation IV reactor design neutrons of up to

10 MeV can be important, and this is the region where the PFGS characteristics are least studied.

Furthermore, new PFGS information will also be useful from a fundamental physics point of view, where results can be compared with theoretical predictions to refine fission models. Prompt-fission $\gamma$-ray spectra integrate a large amount of information about the fission process. Measurements, namely, allow further insight into angular momentum generation at scission [2,3]. In addition, they are expected to lead to a better understanding of the competition between neutron and $\gamma$ emission [4–6], and thereby possibly contribute to investigate the mechanism of excitation energy sorting between the two fission partners [7–9].

While recent measurements have focused on thermal-neutron-induced fission [10–12] and spontaneous fission

[13,14], very little PFG information exists for fast-neutron-induced fission [15,16]. In this work PFGS and their average characteristics for fast-neutron-induced fission on $^{238}$U were studied at energies of 1.9 MeV and 4.8 MeV to gain information on the possible energy dependence of PFG characteristics below second chance fission at 6 MeV.

## II. EXPERIMENTAL SETUP

PFGS from fast-neutron-induced fission on $^{238}$U were measured at the Tandem accelerator of the ALTO facility at IPN Orsay, using the LICORNE neutron source [17]. LICORNE generates kinematically forward-focused neutrons using inverse kinematics reactions of $p(^7\text{Li}, n)^7\text{Be}$, and $p(^{11}\text{B}, n)^{11}\text{C}$. This allows the placement of $\gamma$ detectors close to the measured sample but still outside the neutron beam. Shielding from source neutrons is thus unnecessary. Furthermore, the fast and thermal neutron backgrounds in the experimental room are very low. In this experiment the $p(^{11}\text{B}, n)^{11}\text{C}$ reaction was used for the first time to extend the energy range of the LICORNE source up to around 7 MeV, which allowed exploration of PFGS characteristics of $^{238}$U at incident neutron energy 4.8 MeV. Employing the more intense neutron-producing reaction $p(^7\text{Li}, n)^7\text{Be}$ at lower energies allowed the same study at incident neutron energy 1.9 MeV.

The neutron spectra seen by the samples vary slightly as a function of the solid angle covered due to the inverse kinematics of the reaction. The determination of the incident neutron energy on the $^{238}$U samples thus relies on the simulation of the inverse kinematics inside the hydrogen gas target, which has been implemented in GEANT4, and a subsequent validation using a neutron TOF measurement at 1.5 meters from the LICORNE source. A cylindrical NE213 liquid scintillation detector from the EDEN array [18] was used to perform such measurements. The neutron spectra seen by the samples were simulated for each inverse kinematics reaction and were validated by a comparison between simulated and measured TOF spectra, see Fig. 1. Averaged incident neutron energies on the samples were thus deduced to be $1.9 \pm 0.27$ MeV and $4.8 \pm 0.20$ MeV, respectively. Two neutron peaks are present in the TOF spectra due to the inverse kinematics (forward and backward emission of neutrons in the center of mass frame).
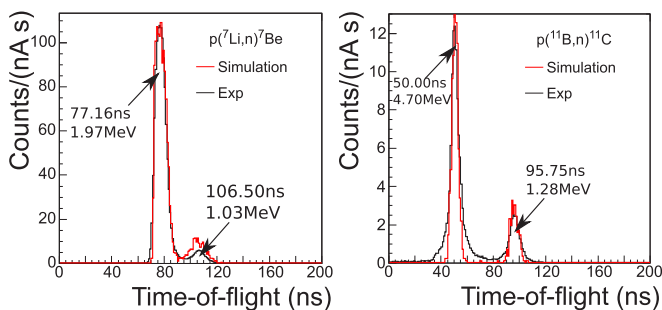


FIG. 1. Measured TOF spectra in the EDEN scintillation detector at zero degrees for the two neutron-producing reactions with LICORNE using a pulsed primary beam of 400 ns period and 2 ns width. The arrival of neutrons in the EDEN scintillation detector gives the start signal and the beam pulsing signal provides the stop signal.

For the case of neutron-induced fission of $^{238}$U, the fission threshold is around 1.4 MeV and thus the smaller satellite peak has an insignificant contribution to the total fission rate because it is below the fission threshold.

In order to detect fission fragments, two fission chambers were constructed at CEA Bruyeres-le-Chatel and used to study prompt emission in fission [19]. The first chamber contained one cathode supporting a 25 mm diameter $^{252}$Cf sample. $^{252}$Cf is a spontaneous fission source that has been widely studied, and measured PFGS can be used as a reference to compare with other results and validate the analysis procedure. The second chamber contained 340 mg uranium samples in 72 deposits ($\oslash = 33$ mm) with a compact geometry (see Fig. 2 for a schematic view). The uranium was deposited on both sides of each anode and cathode, except the first and last samples, which were only coated on the internal side. The anodes are paired two by two constituting nine channels for readout of fission fragment detection information. The chambers have been designed with thin aluminium walls to minimize scattering of prompt $\gamma$ rays and neutrons emitted in fission and thus have minimum distortion of the $\gamma$ and neutron spectra. The key characteristics are the subnanosecond time resolution (732 ps) and excellent discrimination between fission fragments and $\alpha$ particles.

Prompt-fission $\gamma$ rays emitted from fission fragments within the chambers were measured using three types of fast scintillation detectors: seven individual cerium-doped lanthanum bromide LaBr$_3$(Ce), a cluster of nine phoswich detectors from the PARIS array [20], and a cluster of seven barium fluoride BaF$_2$ from the Chateau de Cristal array [21]. The state-of-the-art scintillation detectors made of LaBr$_3$(Ce) (50.8 mm × 50.8 mm and 76.2 mm × 76.2 mm in diameter and length) have excellent time resolution (300 ps for coincidence $\gamma$-rays from $^{60}$Co) and good energy resolution (3% at 661 keV). These detectors were used in several recent measurements of PFGS from different fissioning systems [10,11,13,14] and are used in this work as the main reference detectors to facilitate the comparison. The BaF$_2$ scintillators had a high detection threshold at around 400 keV so results from these detectors are excluded from the analysis and not presented in this work. However, their presence had to be included in the simulations of the experimental geometry from which $\gamma$-ray responses for all the other detectors were derived.

PARIS is an array of a new type of LaBr$_3$(Ce)-NaI(Tl) phoswich detectors. The inner shell is LaBr$_3$(Ce) cubic crystals (50.8 mm × 50.8 mm × 50.8 mm) and the outer shell consists of NaI(Tl) rectangular crystals (50.8 mm × 50.8 mm × 152.4 mm). Both crystals are encapsulated in an aluminium can, sharing one common photomultiplier tube. According to the difference of the decay times of the phoswich material, it is possible to apply pulse shape discrimination (PSD) to differentiate events occurring in the two layers. In this way, PARIS phoswich detectors benefit from superior energy and time resolution of the LaBr$_3$(Ce) part, and increased efficiency, particularly at high energy, from the NaI(Tl) part with lower economical cost than pure LaBr$_3$(Ce) of identical size.

Detector signals were processed using the digital acquisition system FASTER [22] developed by LPC Caen. The system provides QDC cards with 12 bits and a sampling rate of 500 MS/s.
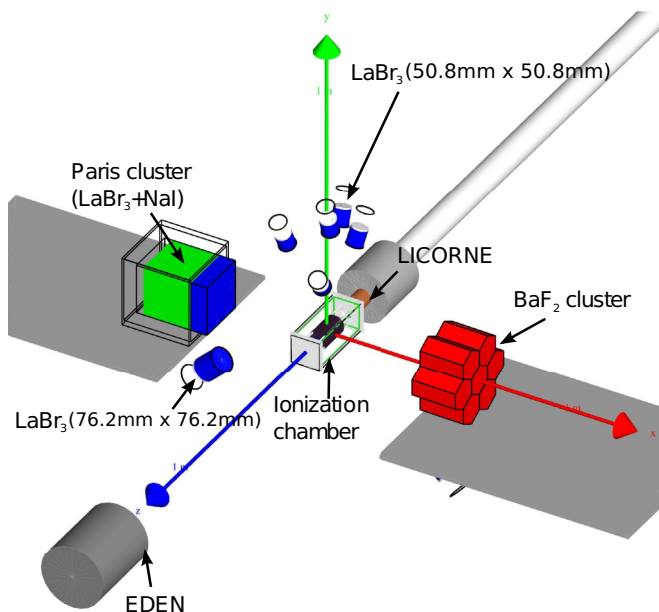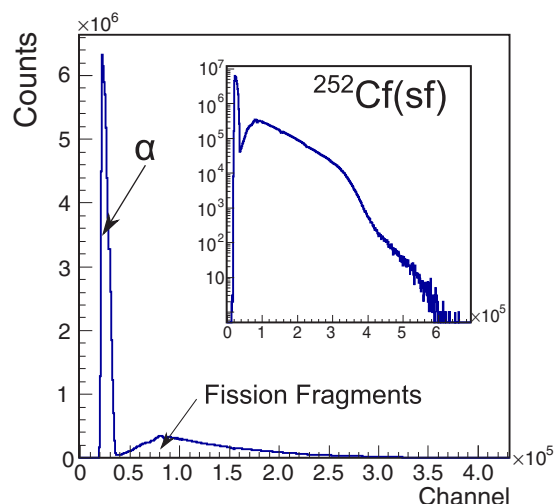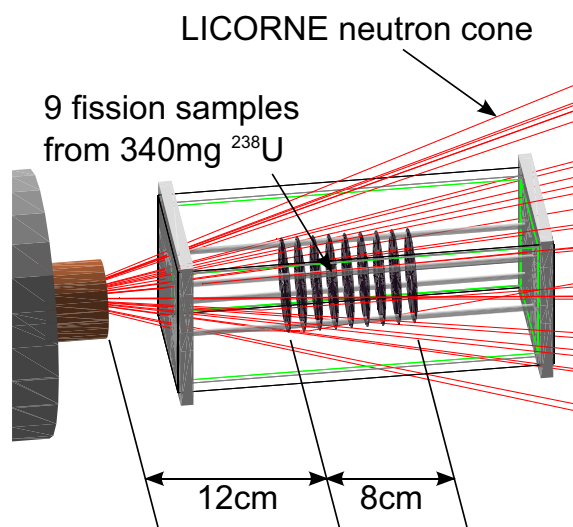
FIG. 3. The integrated charge spectrum taken with the CEA multisample ionization chamber depicted in linear scale; the inset shows the same distribution in logarithmic scale. In both representations, the separation between fission fragments and $\alpha$ particles is visible.

FIG. 2. Schematic of the experimental setup. A cluster of nine phoswich detectors PARIS on the left. A cluster of seven BaF$_2$ detectors on the right. Seven LaBr$_3$(Ce) detectors with two kinds of size in the top and bottom. All these detectors are close to 90 degrees with respect to the beam axis at a distance around 35 cm relative to the ionization chamber.

## III. DATA ANALYSIS

### A. Fission events selection

Fission events were identified from the charge spectrum of the ionization chamber. The separation between charge distributions of fission fragments (ff) and $\alpha$ particles is excellent and hence a very low threshold can be set to select the fission events. The threshold to select fission events from $\alpha$ particles is set at the minimum of the valley between

the two distributions, in this case at channel $36 \times 10^3$ in the spectrum shown in Fig. 3. The number of $\alpha$ particles in the selected fission fragment distribution is estimated by extrapolation to be less than 0.5% and thus induces negligible influence on the measured prompt-fission $\gamma$-ray spectrum. PFGS are then normalized to the total number of fissions to give average spectral characteristics per fission. The total number of fission events detected for fast-neutron-induced fission of $^{238}$U is $1.4 \times 10^6$ and $3.3 \times 10^5$ fissions at neutron energies of 1.9 MeV and 4.8 MeV, respectively. This is one and two orders of magnitude lower than the number of fissions detected in the $^{252}$Cf spontaneous fission measurement ($3.7 \times 10^7$ fissions).

### B. PFG selection

Prompt-fission $\gamma$ rays and prompt-fission neutrons are discriminated using the TOF technique over each chamber-detector distance of typically 35 cm, at which 10 MeV prompt neutrons travel 8 ns. A two-dimensional plot of the TOF between the ionization chamber and the $\gamma$ detector versus detected $\gamma$ energy is shown in Fig. 4. The intense sharp component corresponds to prompt-fission $\gamma$ rays, and defines the zero time reference. The broad component at larger TOF is associated with prompt-fission neutrons, which needs to be in essence eliminated in the prompt $\gamma$ rays spectroscopy. Delayed $\gamma$ lines starting from the prompt $\gamma$ peak can also be seen, and are associated with isomeric decays of particular fission fragments, e.g., 1769 keV $\gamma$ line with lifetime 54 ns can be a candidate for $^{146}$Ce [23]. Other lines originate from neutron inelastic scattering $(n, n'\gamma)$ on materials inside the detectors, e.g., $\gamma$-ray decay of the first excited states of $^{139}$La (165.86 keV), $^{79}$Br (217.07 keV), and $^{81}$Br (275.99 keV), or materials close to the $\gamma$ detectors and the ionization chamber, e.g., $\gamma$-ray decay of the first excited states of $^{27}$Al (843.76 keV) and $^{56}$Fe (846.78 keV). A continuous $\gamma$ background exists along the whole axis associated with uncorrelated decays in
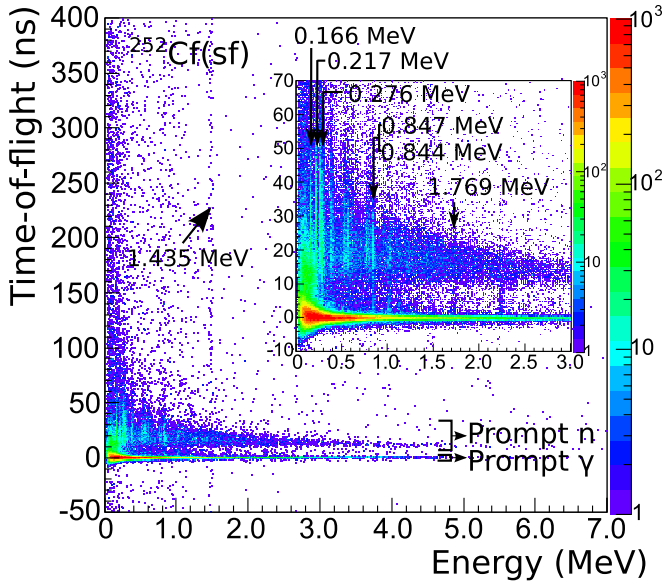
FIG. 4. Correlation between the $\gamma$-ray energy detected in one $\gamma$ detector and the TOF, where the ionization chamber gives the start signal and a $\gamma$ detector gives the stop signal. The inset shows the same correlation in low-energy part. The time resolution, i.e., full width half maximum (FWHM), of the prompt $\gamma$ peaks projected to $y$ axis is around 1.2 ns for each $\gamma$ detector. Gating with a proper time window around zero time reference and applying background subtraction gives the measured PFGS. The choice of the proper time window is discussed in the text.

the experimental room, e.g., 1435.8 keV intrinsic $\gamma$ line from the electron capture on $^{138}$La in LaBr$_3$ detectors. Gating on the time window before the prompt $\gamma$ peak and after the prompt neutron peak allows extraction of this averaged continuous background, which must be normalized and subtracted from the measured PFGS.

In comparison of PFG data with other experimental results and model calculations, two conditions have to be considered in the PFG selection: the size of the time window and the energy range. The size of the time window used to select PFG is crucial, as illustrated in Fig. 5 for the average $\gamma$-ray multiplicity. Since the time resolution is worse at low energies, more stringent cuts disproportionately affect this part of the spectrum and can have large effects on the extracted average multiplicity. For comparison with other experimental results, the time window in this work has been set to 5 ns corresponding to 4 times the FWHM of the time resolution of the prompt $\gamma$ peak. Also, it is sensitive to the energy threshold, since the threshold effect and the massive x rays cannot be well simulated for recovering the emission PFGS, that is going to be discussed in the next section. On the other hand, the high-energy cut is of little relevance to the spectral characteristics due to the exponentially decreasing high-energy yield. As a consequence, the energy range was set from 100 keV–6 MeV. Based on these two conditions, the average number of fission-$\gamma$ coincidences obtained in each detector is $3.1 \times 10^4$ and $7.0 \times 10^3$ for fast-neutron-induced fission of $^{238}$U at neutron energies of 1.9 MeV and 4.8 MeV, which is one and two orders of magnitude lower than the number detected in the
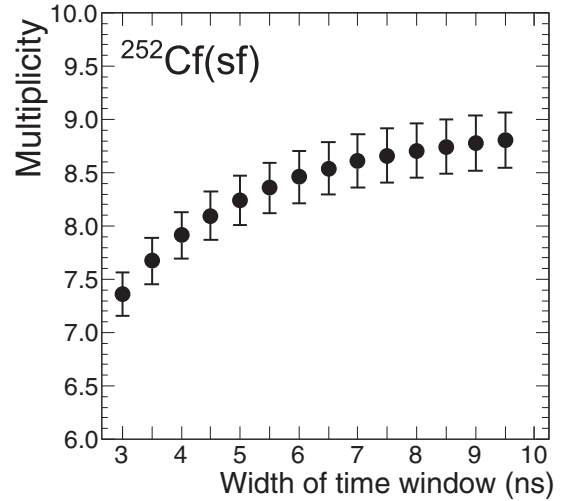


FIG. 5. $\gamma$-ray multiplicity per fission as a function of the size of the time window over which $\gamma$ rays are selected. The data refer to spontaneous fission of $^{252}$Cf.

$^{252}$Cf spontaneous fission measurement ($5.1 \times 10^5$ fission-$\gamma$ coincidences).

### C. Unfolding procedure

In this section, information on the unfolding procedure is given in some detail in order to understand any potential systematic errors that it can introduce. This is especially important for spectra with low statistics, which can be the case for PFG measurements from fast-neutron-induced fission, because cross sections are typically three orders of magnitude lower than those for thermal-neutron-induced fission.

The true emitted PFGS is convoluted with the intrinsic response of the $\gamma$ detectors, mainly due to Compton scattering, photoelectric effect, and pair production. Therefore, the measured spectrum must first be deconvoluted from the detector response to obtain the emission spectrum. Let $f(y)$ to be the unknown emission $\gamma$-ray spectrum of the source, and $R(x, y)$ to be the response matrix. Then

$$g(x) = \int_0^\infty R(x, y) f(y) dy \qquad (1)$$

is the measured spectrum. The challenge is to solve this linear integral equation in order to obtain the emission spectrum $f(y)$ given the measured spectrum $g(x)$ and simulated response function $R(x, y)$, from which the characteristics of each fission event are extracted. This process is called unfolding or deconvolution. It is well known for being an ill-posed problem [24]. In this specific physical case of unfolding PFGS, a detailed procedure is presented in the following sections.

#### *1. Emission spectrum shape*

In the case of PFGS, there is no functional form for the emission spectrum due to the complexity of the process producing the $\gamma$ rays. In its low-energy part (<1 MeV), the spectrum is dominated by discrete (mainly $E2$) transitions, characteristics for the population of low-lying states in fission
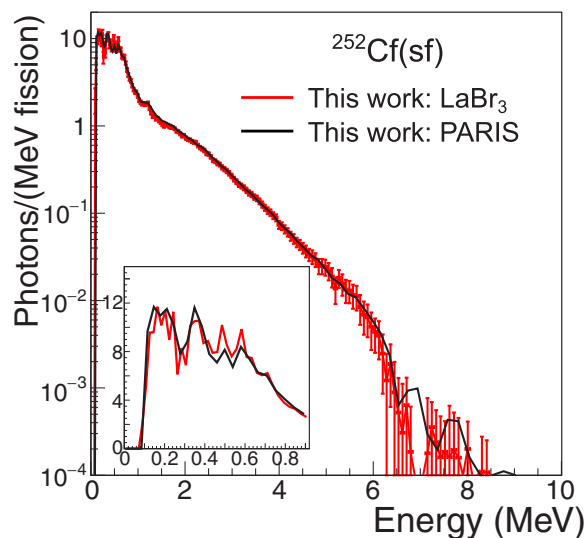
FIG. 6. Averaged unfolded spectra with the time window $\pm 2.5$ ns from $^{252}$Cf($sf$) in logarithmic scale as obtained for two different types of $\gamma$ detectors (see text for details). The error bar of PARIS is omitted for better visibility. The inset shows the region below 900 keV in linear scale.

fragments [25], see inset of Fig. 6. These low-energy $\gamma$ rays sit on a continuous background of statistical $\gamma$ rays, which are mainly $E1$ transitions. The latter cover a wide range of energies from a few tens keV up to 10 MeV. At even higher energies, the deexcitation of giant resonance (GR) of the fragments may be observed [26,27]. In the case of fast-neutron-induced fission, where the cross section is three orders of magnitude lower than thermal-neutron-induced fission, the limited statistics above 6 MeV constrain the study of high-energy $\gamma$ rays (see Fig. 6). In a word, the unfolding task in this experiment cannot be based on *a priori* functional form for the emission spectrum, but the measured spectrum is unfolded directly with the help of the response matrix $R(x, y)$.

### *2. Response matrix construction*

The response matrix itself is obtained from detailed GEANT4 simulations of the entire experimental setup using the PENE-LOPE physics list [28]. In the low-energy part, the threshold has been set at 100 keV to exclude the intense x rays, which cannot be simulated very well. A full energy range up to 10 MeV is used to take into account the effect of Compton scattered high-energy $\gamma$ rays appearing in the lower-energy region of the spectrum. A validation of the response matrix was performed using the detection efficiencies and comparisons between simulated and experimental spectra from conventional $\gamma$ sources, as depicted in Fig. 7.

### *3. Unfolding algorithms*

Various unfolding algorithms for recovering the emission PFGS have been developed over the last 50 years. However, there is a lack of knowledge about what kind of systematic effects the different unfolding algorithms have on the unfolded spectrum, especially the spectral characteristics. In addition,
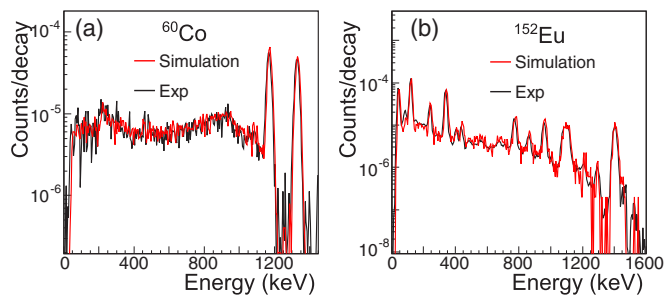


FIG. 7. Comparisons between simulation and experimental results in the case of (a) $^{60}$Co and (b) $^{152}$Eu radioactive source for one LaBr$_3$ detector.

the performance of the unfolding procedures needs to be evaluated in low-statistics data sets, which is particularly relevant for fast-neutron-induced fission PFG measurements. By artificially reducing the number of events, the impact of low statistics on the extracted average multiplicity has been quantified for each unfolding algorithm, including matrix inversion, bin by bin [29], Tikhonov regularization [30], singular value decomposition (SVD) regularization [31], linear and nonlinear iteration method [32,33]. The results, shown in Fig. 8, demonstrate that the iteration method is the most stable for spectra with the fewest counts. As a consequence, linear iteration algorithm is used in this work.

### *4. Observables extraction*

Once the unfolding is completed, the spectral characteristics can then be extracted from the unfolded spectra, which are normalized to the number of fissions. The average multiplicity is deduced by integrating the unfolded spectrum. The multiplication between the unfolded distribution and the $\gamma$-ray energy gives the total energy released. The average photon energy can
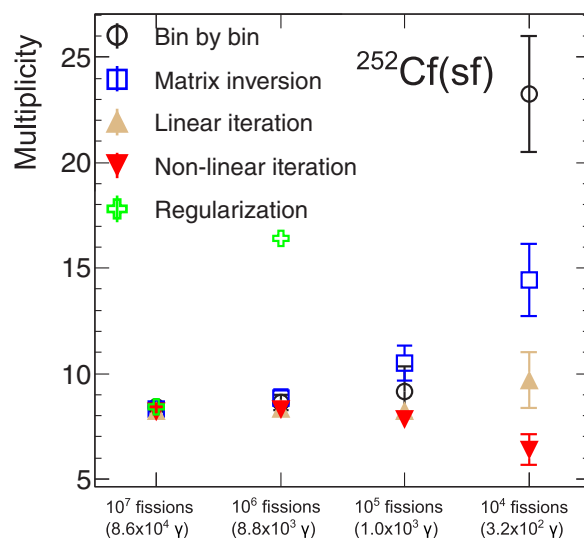


FIG. 8. Comparison of different unfolding techniques from the spontaneous fission source $^{252}$Cf at different statistical configurations, with the extracted property of $\gamma$-ray multiplicity per fission.
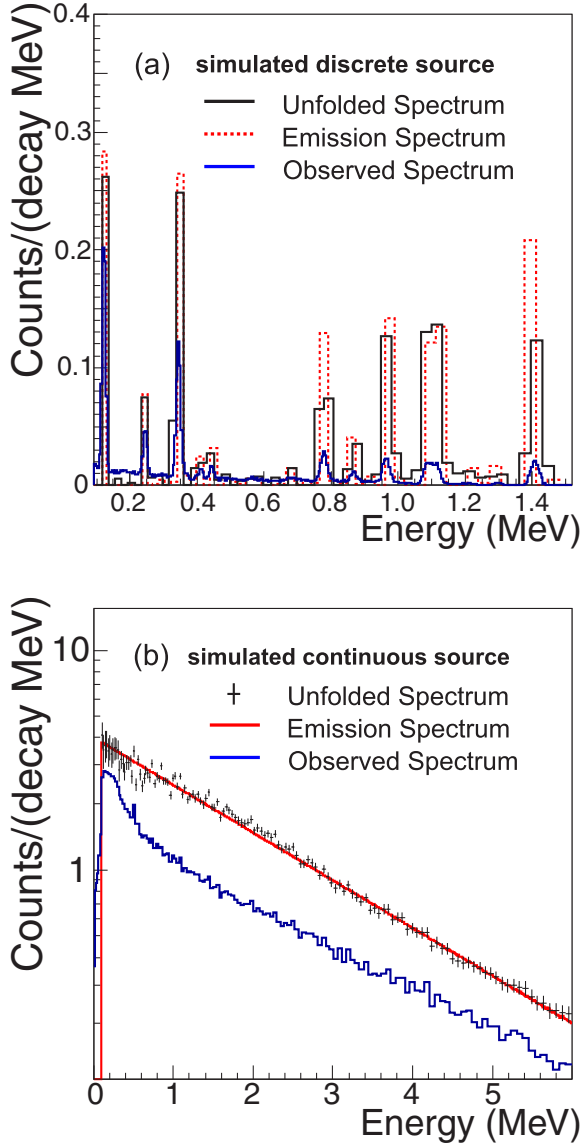
TABLE I. Summary of the spectral characteristics for unfolded spectrum and emission spectrum.

| | | $\overline{M}_\gamma$ | $E_{\gamma,\text{tot}}$ (MeV) | $\epsilon_\gamma$ (MeV) |
|---|---|---|---|---|
| $^{152}$Eu source | unfolded | $1.65 \pm 0.06$ | $1.16 \pm 0.02$ | $0.70 \pm 0.03$ |
| | emission | $1.58 \pm 0.01$ | $1.11 \pm 0.00$ | $0.71 \pm 0.01$ |
| exponential | unfolded | $7.28 \pm 0.08$ | $12.93 \pm 0.07$ | $1.77 \pm 0.02$ |
| | emission | $7.25 \pm 0.02$ | $12.86 \pm 0.00$ | $1.77 \pm 0.00$ |

which causes oscillation in the neighboring bins, the spectral characteristics of the unfolded spectrum very well represent those of the emission spectrum, as summarized in Table I. The analysis also shows that, for one detector, aforementioned linear-iteration unfolding procedures reasonably reproduce the average multiplicity, the total energy released, as well as the average photon energy, here applied to a high-statistics data sets.

## IV. RESULTS

### A. $^{252}$Cf($sf$) data

In order to validate the data analysis procedure, PFGS from a $^{252}$Cf spontaneous fission source were measured since $^{252}$Cf has been extensively studied and is very useful as an evaluated standard. The measured spectrum of each individual $\gamma$ detector was unfolded separately, following the unfolding procedure discussed in the preceding section. The spectral characteristics are then extracted individually. The final values are obtained from the weighted mean and associated uncertainties of spectra from the multiple detectors in the experimental setup. The values obtained are presented in Table II. Each individual unfolded spectrum from multiple detectors was combined into two averaged unfolded spectra for different detector types, i.e., LaBr$_3$ scintillation detector and PARIS phoswich detector, as is plotted in Fig. 6.

The unfolded spectra (Fig. 6) from the LaBr$_3$ scintillation detectors and the PARIS phoswich detectors are in very good agreement with each other despite the very different $\gamma$-ray responses. There is good agreement in terms of both the slope in the high-energy region and the positions of the structures in the low-energy region. There are some small differences observed in the amplitude of the major peaks in the low-energy region, but this may be due to the different energy resolutions of the two detector types and are also within the uncertainties. The spectral characteristics for the two types of the detectors agree



FIG. 9. Comparison of the unfolded $\gamma$-ray spectra for (a) a discrete $\gamma$ source $^{152}$Eu and (b) an exponentially distributed $\gamma$ source. Each unfolded spectrum is compared to the emission spectrum, as well as the measured spectrum (scaled for better visibility).

then be calculated from these two quantities,

$$\overline{M}_\gamma = \int N_\gamma(E_\gamma)\,dE_\gamma \tag{2}$$

$$E_{\gamma,\text{tot}} = \int E_\gamma \times N_\gamma(E_\gamma)dE_\gamma \tag{3}$$

$$\epsilon_\gamma = E_{\gamma,\text{tot}}/\overline{M}_\gamma. \tag{4}$$

In order to validate the calculations, simulated data with high statistics are used in case of a discrete (radioactive source $^{152}$Eu) and a continuous (energy in exponential, multiplicity in Gaussian) distribution, which are typical for PFGS. Figure 9 gives the comparison among measured spectrum, unfolded spectrum, and emission spectrum. Even though the unfolded spectrum cannot fully eliminate the energy shearing effect,

TABLE II. Summary of PFGS characteristics for the $^{252}$Cf spontaneous fission source.

| | $\overline{M}_\gamma$ | $E_{\gamma,\text{tot}}$ (MeV) | $\epsilon_\gamma$ (MeV) |
|---|---|---|---|
| This work: LaBr$_3$ | $8.30 \pm 0.15$ | $6.60 \pm 0.15$ | $0.80 \pm 0.02$ |
| This work: PARIS | $8.40 \pm 0.19$ | $6.70 \pm 0.26$ | $0.80 \pm 0.02$ |
| Billnert *et al.* [29] | $8.30 \pm 0.09$ | $6.64 \pm 0.10$ | $0.80 \pm 0.01$ |
| Chyzh *et al.* [34] | $8.14 \pm 0.40$ | $7.65 \pm 0.55$ | $0.94 \pm 0.05$ |
| ENDF/B-VII.1$^a$ [35] | 7.79 | 6.70 | 0.86 |

$^a$Energy range: 0.1–6.0 MeV.

TABLE III. Summary of PFGS characteristics for the $^{238}$U$(n, f)$ reaction at different incident neutron energies.

| | $E_n$ (MeV) | $\overline{M}_\gamma$ | $E_{\gamma,\text{tot}}$ (MeV) | $\epsilon_\gamma$ (MeV) |
|---|---|---|---|---|
| LaBr$_3$ | 1.9 | $6.38 \pm 0.19$ | $5.15 \pm 0.21$ | $0.81 \pm 0.04$ |
| | 4.8 | $7.37 \pm 0.49$ | $6.29 \pm 0.69$ | $0.85 \pm 0.11$ |
| PARIS | 1.9 | $6.69 \pm 0.19$ | $5.35 \pm 0.19$ | $0.80 \pm 0.04$ |
| | 4.8 | $7.25 \pm 0.42$ | $6.06 \pm 0.60$ | $0.84 \pm 0.10$ |
| total | 1.9 | $6.54 \pm 0.19$ | $5.25 \pm 0.20$ | $0.80 \pm 0.04$ |
| | 4.8 | $7.31 \pm 0.46$ | $6.18 \pm 0.65$ | $0.84 \pm 0.11$ |
| Laborie *et al.* [15] | 1.7 | $7.05 \pm 0.20$ | $5.92 \pm 0.24$ | $0.84 \pm 0.03$ |
| | 5.2 | $7.25 \pm 0.35$ | $5.73 \pm 0.40$ | $0.79 \pm 0.04$ |

well within 1.5% and are within the error bars (see Table II). This demonstrates a good performance of the PARIS phoswich detectors in this experiment—in fact, the first time that these detectors have been used in a real physics measurement.

Our results from $^{252}$Cf are also in very good agreement with results from previous experiments [29,34] and evaluated databases [35]. Comparisons are given in Table II. We conclude that our analysis procedure is validated and may now be applied to the spectral data obtained in our measurements of PFG from neutron-induced fission of $^{238}$U$(n, f)$, as presented in the next section.

## B. $^{238}$U$(n, f)$ data

In this section we present the experimental PFGS results from fast-neutron-induced fission of $^{238}$U at two different incident energies (1.9 and 4.8 MeV) to examine any potential energy dependence of spectral characteristics below second chance fission. The $^{238}$U ionization chamber used for the measurement had an identical external geometry and was constructed of similar materials compared to the $^{252}$Cf chamber. However, the samples in the $^{238}$U chamber were positioned between 12 and 20 cm from the source covering slightly different solid angles. For the $^{238}$U$(n, f)$ case, the response matrix for each $\gamma$ detector has to be simulated at nine different positions (see Fig. 2) taking into account the corresponding change in source geometry. The measured PFGS corresponding to each fission position have been unfolded separately. To obtain the final values for the spectral characteristics, i.e., average multiplicity, total energy release, and average photon energy, each spectrum was analyzed independently and used to extract weighted means for each of the relevant quantities, see Table III. To obtain the final unfolded spectrum in Fig. 10, all the separate unfolded spectra for each detector and each of the nine source positions, were combined into two averaged unfolded spectrum for different detector types.

A linear fit to the spectral characteristics for the two incident neutron energies in this work has been performed. For example, the trend of the total energy released per fission has a slope $0.32 \pm 0.14$ MeV/MeV and an intersection $4.64 \pm 0.32$ MeV. The experimental results reveal that the spectral characteristics of PFGS, including the average multiplicity, the total energy release as well as the average photon energy, have no significant observable energy dependence when the beam energy is raised
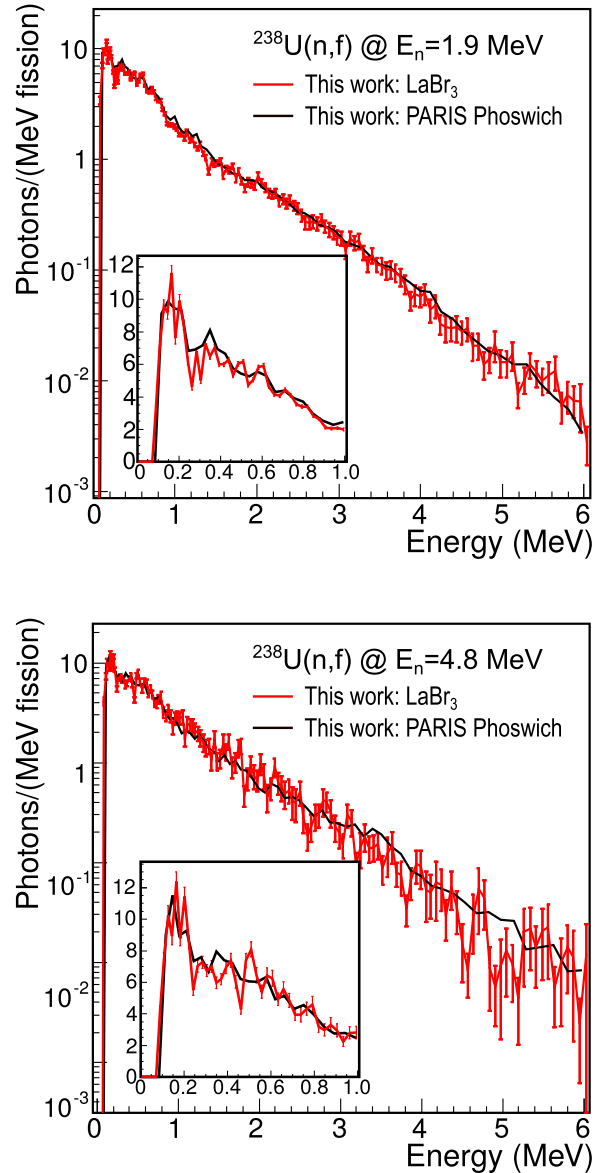


FIG. 10. Averaged unfolded spectra with the time widonw $\pm 2.5$ ns for the $^{238}$U$(n, f)$ reaction in logarithmic scale, as obtained for two different types of $\gamma$ detectors. The error bar of PARIS is omitted for better visibility. The inset shows the region below 900 keV in linear scale.

from 1.9 to 4.8 MeV (see Fig. 11). Also no significant observable evolution in the shape of the spectrum is seen (Fig. 10).

## V. DISCUSSIONS

Changes in the PFG characteristics with incident neutron energy can occur due to two different effects. The first is through changes in the fission yields where the relative contributions from each fission fragment depends on the incident neutron energy. The second is from the extra total fragment excitation energy (TXE) available for both neutron and $\gamma$ emission.
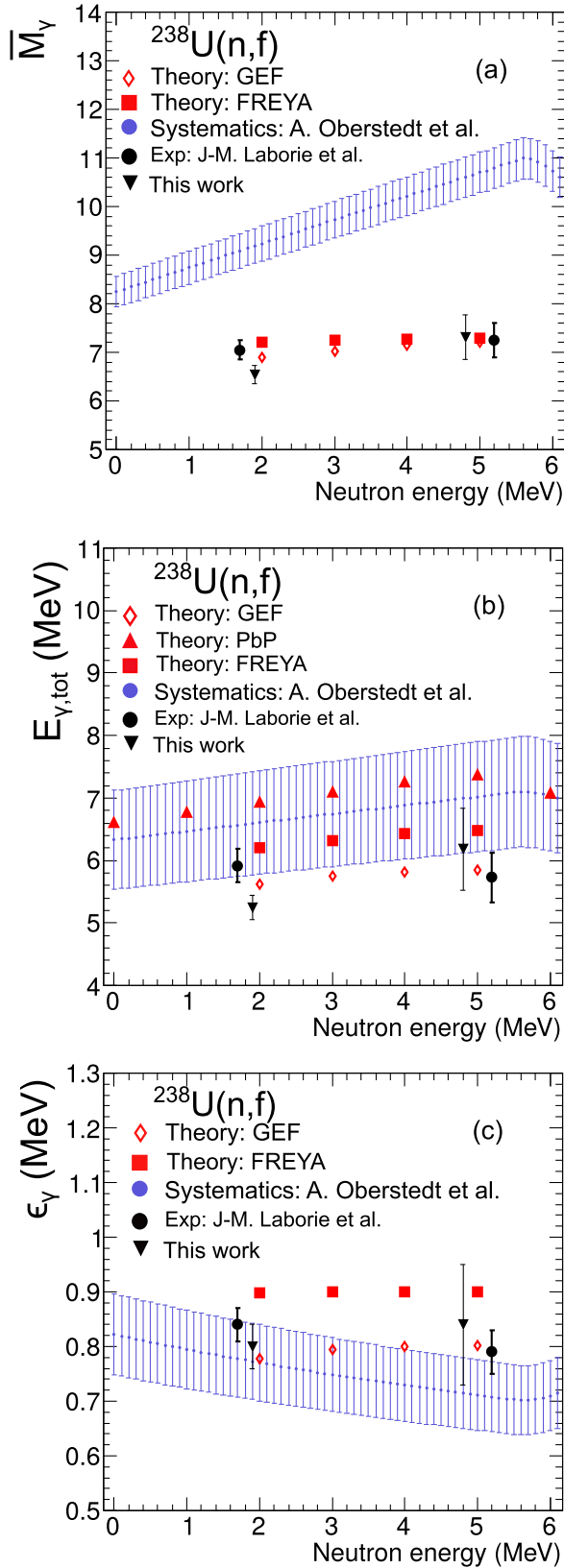
FIG. 11. Summary of the PFGS characteristics: (a) average multiplicity $\overline{M}_\gamma$; (b) average total energey $E_{\gamma,\mathrm{tot}}$; (c) average $\gamma$-ray energy $\epsilon_\gamma$, as function of neutron energy, for fast-neutron-induced fission of $^{238}$U.

According to the measured mass distributions for this fissioning system [36], the yield of the standard 1 (S1) and standard 2 (S2) modes do indeed change within the present neutron-energy range (S1 decreases from 32.26% to 27.39%, while S2 increases from 67.22% to 71.64%). Hence, it is expected that the low-energy part of the $\gamma$-ray spectrum, where the contribution comes mainly from discrete transitions characteristic of the populated fragments, changes with neutron energy. However, due to the large variety of fragment isotopes and their close-lying $\gamma$ lines, on one side, and the limited energy resolution of scintillation detectors, on the other side, broad structures (rather than sharp peaks) appear in the low-energy part of the spectrum. These correspond to bunched groups of close-lying $\gamma$ lines. Altogether, changes in these structures are expected to be small over the studied neutron energy range, and we are indeed unable to evidence them clearly with the precision of the current measurement.

The change in incident neutron energy in this experiment leads to an extra 2.90 MeV of excitation energy imparted to the $^{239}$U* compound nucleus, which is shared between the total kinetic energy (TKE) and TXE of fission fragments. Previous measurements [37] have shown that the average TKE is decreased by 1.33 MeV when the incident neutron energy is increased from 1.9 to 4.8 MeV for this fissioning system. Hence, an extra 4.23 MeV of TXE is available for neutron and $\gamma$ emission based on the energy balance as follows:

$$\overline{TXE} = \overline{\nu}_n(\overline{\epsilon}_n + \overline{S}_n) + E_{\gamma,\mathrm{tot}}, \qquad (5)$$

where $\overline{\nu}_n$ is the average neutron multiplicity, $\overline{\epsilon}_n$ is the average neutron energy, and $\overline{S}_n$ is the average neutron separation energy. The average neutron multiplicity $\overline{\nu}_n$ changes from 2.57 to 2.98 and the average neutron energy $\overline{\epsilon}_n$ from 1.78 to 1.81 MeV according to the JEFF-3.3 evaluated library [38] in this energy range. The average neutron separation energy $\overline{S}_n$ is estimated to change from 4.80 to 4.86 MeV, when calculated using experimental masses [39] or theoretical masses [40] and weighted by the fission yields obtained from GEF [41]. According to the $E_{\gamma,\mathrm{tot}}$ obtained from this work in Table III, a TXE of $22.16 \pm 0.20$ MeV and $26.06 \pm 0.65$ MeV (only the uncertainty of $E_{\gamma,\mathrm{tot}}$ is considered) are obtained for $E_n = 1.9$ MeV and $E_n = 4.8$ MeV, respectively. It gives rise to an increase of $3.9 \pm 0.68$ MeV in TXE, which is reasonably well in agreement with the aforementioned 4.23 MeV of extra TXE. This suggests that $(76 \pm 13)\%$ of the excess energy is evacuated by neutron evaporation and $(24 \pm 18)\%$ for the photon emission, which means that the majority of the extra available TXE is dissipated by prompt-fission neutron (PFN) emission. Despite the weaker increase of PFG emission relative to PFN emission, our results suggest that the assumption that neutron emission entirely precedes $\gamma$ emission, is not valid and that competition of both play a considerable role during the deexcitation of fission fragments [4–6].

Figure 11 contains—as a function of incident neutron energy—the average values for each quantity from this work, together with results from various fission models, including PbP [42], GEF [41], and FREYA [43], as well as calculations based on systematics [44]. The calculated observables of PFG from GEF and FREYA have reasonable agreement with the experimental results and also exhibit a slightly increasing
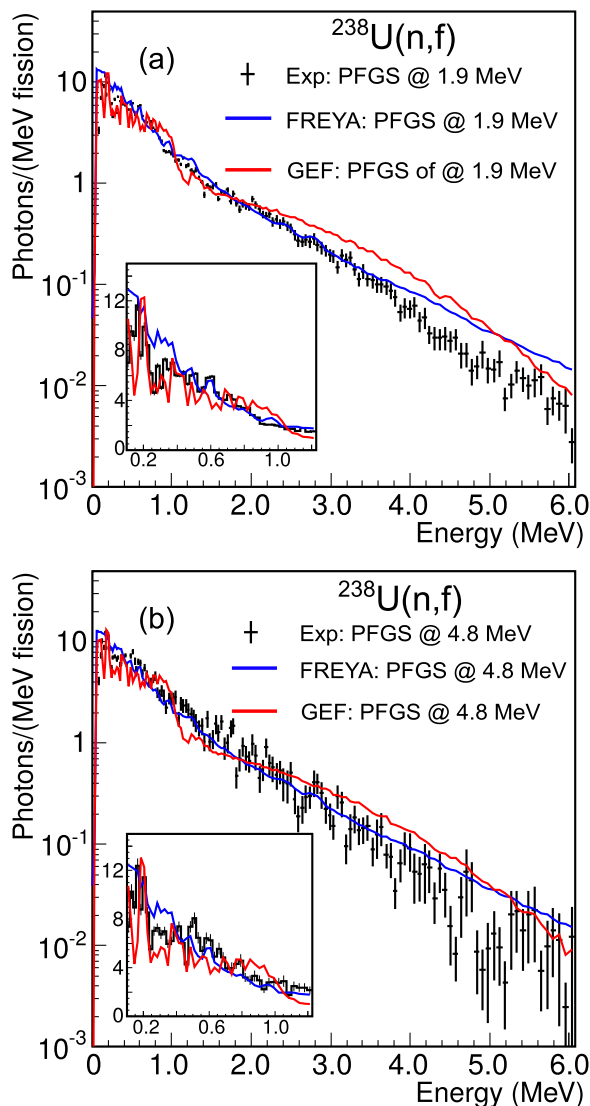
FIG. 12. (a) and (b) Comparison between the unfolded PFGS of this work (LaBr$_3$) and the calculation from FREYA and GEF at two incident neutron energies, respectively.

trend in terms of average $\gamma$ multiplicity and total energy per fission. Some discrepancies are observed in the calculations based on systematics for the $^{238}$U$(n, f)$ reaction. We report much lower average $\gamma$ multiplicity per fission, slightly lower total energy, and higher average energy per fission, compared to the calculations based on systematics. A possible reason for the discrepancies is that these calculations are based on the assumption that the average total $\gamma$-ray energy is linearly depending on the neutron multiplicity. In addition it highly relies on the fit with respect to the experimental PFG data to get the coefficients, where the number of experimental PFG data are still clearly insufficient.

A detailed comparison in terms of PFGS for our experiment, FREYA, and GEF model calculations, is performed in Fig. 12. Both model calculations, from GEF and FREYA, can reasonably describe our experimental spectra and do not show significant differences at the two incident neutron energies.

However, the enhanced yield above 3 MeV calculated with the GEF code is not supported by our experimental results. Even though the calculation for $E_n = 4.8$ MeV is closer to the experimental data, the spectral slope does not, despite the larger statistical uncertainty, support the enhanced calculated yield above $E_\gamma = 3$ MeV.

Our observation of at most weak energy dependence of the PFG characteristics in this energy range is, within uncertainties, compatible with the results of Laborie *et al.* [15]. It is also of importance for nuclear applications, since $\gamma$-ray heating accounts for a major source of energy deposition in certain reactor components, e.g., instrumentations and structural materials. In particular, the heating from $\gamma$ rays is two orders of magnitude higher than neutron heating [45] in reactor reflectors and shielding, and needs to be estimated to a reasonable accuracy to avoid possible fracture and failure. The observed results facilitate the design for the fast reactors in Generation IV, which may not require significant changes in the modeling of $\gamma$ heating transportation.

## VI. CONCLUSIONS

Prompt-fission $\gamma$-ray spectra have been measured for the $^{238}$U$(n, f)$ reaction using fast neutrons of energies 1.9 MeV and 4.8 MeV with the directional neutron generator LICORNE using the $p(^7$Li$, n)^7$Be and $p(^{11}$B$, n)^{11}$C reactions. After correction of the measured spectra for the detection system response via an unfolding procedure, the emitted spectra could be obtained and average spectral characteristics were extracted. Different unfolding techniques were applied, demonstrating the importance of a proper choice of the unfolding methods, particularly in the case of low-statistics spectra. A validation of the measurement was made by a corresponding reference measurement of the PFGS characteristics for the spontaneous fission of $^{252}$Cf, where results were in very good agreement with previous experiments. It reinforces the study of the $^{238}$U$(n, f)$ reaction with lower-statistics data sets. In unfolded PFGS for the $^{238}$U$(n, f)$ reaction at two incident neutron energies, there is no evidence for a firm shape change of the PFGS within the precision of the measurement. Additionally, no significant energy dependence for the spectral characteristics of PFGS below the second chance fission has been observed. Our results provide important information on PFGS characteristics for fast-neutron-induced fission in general, and belong to the first ever experimental data for the fissioning system of $^{239}$U*, complementing previous measurements on thermal-neutron-induced fission and spontaneous fission.

[1] Nuclear Data High Priority Request List of the NEA (Req. ID: H.3, H.4); http://www.nea.fr/html/dbdata/hprl/hprlview.pl?ID=421 and http://www.nea.fr/html/dbdata/hprl/hprlview.pl?ID=422

[2] D. C. Aumann, W. Gükel, E. Nirschl, and H. Zeising, Phys. Rev. C **16**, 254 (1977).

[3] L. G. Moretto and R. P. Schmitt, Phys. Rev. C **21**, 204 (1980).

[4] H. Nifenecker, C. Signarbieux, M. Ribrag, J. Poitou, and J. Matuszek, Nucl. Phys. A **189**, 285 (1972).

[5] D. L. Bleuel *et al.*, Nucl. Instrum. Methods Phys. Res., Sect. A **624**, 691 (2010).

[6] T. Wang *et al.*, Phys. Rev. C **93**, 014606 (2016).

[7] S. Lemaire, P. Talou, T. Kawano, M. B. Chadwick, and D. G. Madland, Phys. Rev. C **72**, 024601 (2005).

[8] O. Litaize and O. Serot, Phys. Rev. C **82**, 054616 (2010).

[9] K.-H. Schmidt and B. Jurado, Phys. Rev. Lett. **104**, 212501 (2010).

[10] A. Oberstedt, T. Belgya, R. Billnert, R. Borcea, T. Brys, W. Geerts, A. Gook, F. J. Hambsch, Z. Kis, T. Martinez, S. Oberstedt, L. Szentmiklosi, K. Takacs, and M. Vidali, Phys. Rev. C **87**, 051602(R) (2013).

[11] A. Gatera, T. Belgya, W. Geerts, A. Gook, F. J. Hambsch, M. Lebois, B. Maroti, A. Moens, A. Oberstedt, S. Oberstedt, F. Postelt, L. Qi, L. Szentmiklosi, G. Sibbens, D. Vanleeuw, M. Vidali, and F. Zeiser, Phys. Rev. C **95**, 064609 (2017).

[12] A. Chyzh, C. Y. Wu, E. Kwan, R. A. Henderson, J. M. Gostic, T. A. Bredeweg, A. Couture, R. C. Haight, A. C. Hayes-Sterbenz, M. Jandel, H. Y. Lee, J. M. O'Donnell, and J. L. Ullmann, Phys. Rev. C **87**, 034620 (2013).

[13] S. Oberstedt *et al.*, EPJ Web Conf. **62**, 02003 (2013).

[14] S. Oberstedt, A. Oberstedt, A. Gatera, A. Gook, F. J. Hambsch, A. Moens, G. Sibbens, D. Vanleeuw, and M. Vidali, Phys. Rev. C **93**, 054603 (2016).

[15] J-M. Laborie, G. Belier, and J. Taieb, Phys. Proc. **31**, 13 (2012).

[16] M. Lebois *et al.*, EPJ Web Conf. **122**, 01010 (2016).

[17] M. Lebois *et al.*, Nucl. Instrum. Methods Phys. Res. A **735**, 145 (2014).

[18] H. Laurent *et al.*, Nucl. Instrum. Methods Phys. Res. A **326**, 517 (1993).

[19] J. Taieb, B. Laurent, G. Bélier, A. Sardet, and C. Varignon, Nucl. Instrum. Methods Phys. Res. A **833**, 1 (2016).

[20] A. Maj *et al.*, Acta Phys. Pol. B **40**, 565 (2009).

[21] D. Guillemaud-Mueller, AIP Conf. Proc. **425**, 290 (1998).

[22] http://www.faster.in2p3.fr

[23] C. Gautherin, PhD. Thesis (in French), CEA DAPNIA/SPhN–97-02T (1997), https://inis.iaea.org/search/search.aspx?orig_q=RN:31017434.

[24] P. C. Hansen, Inverse Probl. **8**, 849 (1992).

[25] T. Materna *et al.*, EPJ Web Conf. **146**, 04041 (2017).

[26] H. Van der Ploeg *et al.*, Nucl. Phys. A **569**, 83 (1994).

[27] H. Makii *et al.*, EPJ Web Conf. **146**, 04036 (2017).

[28] B. A. Faddegon *et al.*, Phys. Med. Biol. **54**, 6151 (2009).

[29] R. Billnert, F. J. Hambsch, A. Oberstedt, and S. Oberstedt, Phys. Rev. C **87**, 024601 (2013).

[30] S. Schmitt, JINST **7**, T10003 (2012).

[31] A. Hoecker and V. Kartvelishvili, Nucl. Instrum. Methods Phys. Res. A **372**, 469 (1996).

[32] A. László, J. Phys.: Conf. Ser. **368**, 012043 (2012).

[33] G. Zech, Nucl. Instrum. Methods Phys. Res. A **716**, 1 (2013).

[34] A. Chyzh, C. Y. W., E. Kwan, R. A. Henderson, J. M. Gostic, T. A. Bredeweg, R. C. Haight, A. C. Hayes-Sterbenz, M. Jandel, J. M. ODonnell, and J. L. Ullmann, Phys. Rev. C **85**, 021601(R) (2012).

[35] ENDF/B-VII.1 Evaluated Nuclear Data File ZA = 98252, MF = 15, MT = 18, 2011; http://www.nndc.bnl.gov/exfor/endf11.jsp

[36] F. Vives, F. J. Hambsch, H. Bax, and S. Oberstedt, Nucl. Phys. A **662**, 63 (2000).

[37] D. L. Duke, F. Tovesson, A. B. Laptev, S. Mosby, F. J. Hambsch, T. Brys, and M. Vidali, Phys. Rev. C **94**, 054604 (2016).

[38] JEFF-3.3 Nuclear Data Library ZA = 98252, MF = 5, MT = 18; 456, 2017, https://www-nds.iaea.org/exfor/endf.htm

[39] G. Audi and A. H. Wapstra, Nucl. Phys. A **595**, 409 (1995).

[40] P. Moller, J. R. Nix, W. D. Myers, and W. J. Swiatecki, At. Data Nucl. Data Tables **59**, 185 (1995).

[41] K-H. Schmidt, B. Jurado, C. Amouroux, and C. Schmitt, Nucl. Data Sheets **131**, 107 (2016).

[42] F-J. Hambsch, S. Oberstedt, G. Vladuca, and A. Tudora, Nucl. Phys. A **709**, 85 (2002).

[43] J. Randrup and R. Vogt, Phys. Rev. C **80**, 024601 (2009).

[44] A. Oberstedt, R. Billnert, and S. Oberstedt, Phys. Rev. C **96**, 034612 (2017).

[45] A-C. Colombier *et al.*, EPJ Web Conf. **42**, 04001 (2013).